Shen *et al.*
Chinese Journal of Mechanical Engineering (2022) 35:113
https://doi.org/10.1186/s10033-022-00793-2

Chinese Journal of Mechanical Engineering

ORIGINAL ARTICLE

Open Access

Kinematics Analysis and Singularity Avoidance of a Parallel Mechanism with Kinematic Redundancy

Chaoyu Shen[1,2], Haibo Qu[1,3*], Sheng Guo[1,3] and Xiao Li[1]

Abstract

The kinematic redundancy is considered as a way to improve the performance of the parallel mechanism. In this paper, the kinematics performance of a three degree-of-freedom parallel mechanism with kinematic redundancy (3-DOF PM-KR) and the influence of redundant parts on the PM-KR are analyzed. Firstly, the kinematics model of the PM-KR is established. The inverse solutions, the Jacobian matrix, and the workspace of the PM-KR are solved. Secondly, the influence of redundancy on the PM-KR is analyzed. Since there exists kinematic redundancy, the PM-KR possesses fault-tolerant performance. By locking one actuating joint or two actuating joints simultaneously, the fault-tolerant workspace is obtained. When the position of the redundant part is changed, the workspace and singularity will be changed. The results show that kinematic redundancy can be used to avoid singularity. Finally, the simulations are performed to prove the theoretical analysis.

Keywords: Parallel mechanism, Kinematic redundancy, Singularity, Simulation analysis

1 Introduction

The parallel mechanism is defined as a closed-loop kinematic chain mechanism whose end-effector is linked to the fixed base by several independent kinematic chains [1]. It has some advantages of high stiffness, high accuracy, and small error accumulation. However, it also has some disadvantages, such as singularities in the workspace and difficulty to eliminate self-motion. The self-motion of the parallel mechanism means that when all its actuating joints are locked, the moving platform will produce a certain position or posture change, which proves that the kinematic performance of the mechanism is general. Many scholars have tried to improve the performance of the parallel mechanism by adding redundant actuators or redundant structures.

Scientist Merlet [2] pointed out that redundancy was a way to improve parallel mechanisms' performance. For parallel mechanisms with redundant actuators, the number of actuators is greater than the number of the mobility of the parallel mechanism. Many researchers proved that redundant actuators could be used to solve the forward kinematics [3], avoid singularities [4, 5], and optimize the distribution of force torque [6–8]. However, the redundant actuators need strict movement coordination, which increases the control difficulty.

In order to overcome the shortcomings and realize the self-coordination between inputs and outputs, some scholars proposed to design parallel mechanisms with redundant kinematic structures. For the general parallel mechanism, the actuating joints, the mobility of the mechanism, and the DOFs of the moving platform are equal in number. However, for a parallel mechanism with kinematic redundancy, the number of mobility is equal to the number of actuators but it is greater than that of the DOF of the moving platform. Besides the earlier studies [9–11], many researchers have played great attention to

*Correspondence: hbqu@bjtu.edu.cn

[1] Robotics Research Center, School of Mechanical, Electronic and Control Engineering, Beijing Jiaotong University, Beijing 100044, China
Full list of author information is available at the end of the article

the parallel mechanism with kinematic redundancy in recent years.

The Gosselin group conducted a lot of relevant analysis for the kinematically redundant parallel mechanism. Wen et al. [12, 13] proposed a (6+3) DOF kinematically redundant hybrid parallel robot and did a lot of kinematic analysis on it, and the singularities of this mechanism were proved avoidable, indicating that this mechanism had a large workspace. They introduced a new method for detecting mechanical interferences between two links that were not directly connected, proposed for evaluating the workspace of the kinematically redundant parallel mechanism. Landuré et al. [14] proposed a spherical parallel robot and proved that its workspace was huge. The analysis of the mechanism's singularity showed that the kinematically redundant parallel mechanism's workspace had design advantages. Isaksson et al. [15] provided an analysis of a class of kinematically redundant parallel manipulators. They explored the singularity of this kind of parallel mechanism with kinematic redundancy by using the screw theory.

Many researchers explored the type synthesis of the parallel mechanism with kinematic redundancy. Qu et al. [16–18] discussed the difference between a parallel manipulator's mobility and the relative degree of freedom (RDOF). Based on the proposed RDOF criterion, they performed the type synthesis of the parallel manipulator with open-loop limbs or closed-loop limbs. Besides, they synthesized a kind of kinematically redundant parallel manipulator based on the modified G-K formula and RDOF criterion. Li et al. [19] summarized several types of parallel mechanisms with 2R1T redundant parallel mechanisms and 2T1R redundant parallel mechanisms, and the results showed that all kinematic redundant mechanisms had a good performance. Wang et al. [20] proposed a hybrid strategy based on the combination of linear decoupling geometric analysis method and high-order convergence iteration method to solve the positive solution of parallel mechanism.

Studies show that the kinematics redundant parallel mechanism has dramatically improved its kinematic performance in its mechanism singularity and workspace [21–23]. Qu et al. [24] proposed a new 3-RRR parallel mechanism with kinematic redundancy and used three examples to illustrate that the workspace boundary and singular configuration could be changed by adjusting the kinematic redundant actuating parameter. Zhao et al. [25] proposed a 3-RPS/3-SPS parallel mechanism with redundant limbs and defined the evaluation index of the workspace. The results showed that the workspace and kinematics performance of the mechanism were improved. Jin et al. [26] designed a type of 2RIT kinematics redundant parallel mechanism, analyzed the inverse kinematics and workspace of this mechanism, and proved that it had a larger two-dimensional rotation angle of the workspace. Besides, the geometry of the kinematically redundant can be optimized based on the singularity and workspace [27].

For the kinematically redundant parallel mechanism, the influence of redundant kinematics components on the mechanism was explored by solving the statics and dynamics. Qu et al. [28] analyzed the statics of a planar parallel mechanism with kinematic redundancy, and its actuating torque was significantly lower than that of the 3-RRR parallel mechanism. This showed that the introduction of the kinematic redundant components could change the force transmission of the mechanism and improve the statics performance. Bahman et al. [29] took a 3-RPRR planar kinematics redundant mechanism as the research object and used the principle of virtual work to obtain the inverse dynamics of the mechanism. The comparison with the non-redundant mechanism showed that the mechanism could avoid the pass through the rotating joint by adding redundant components. Schreiber et al. [30] studied the dynamic trace planning for a 3-DOF space parallel robot and established its dynamic model. PM-KR has many application prospects, such as solar energy collection devices, 3D simulation equipment, and loading and unloading robots in manufacturing.

The above analysis proves that adding kinematic redundant components to the parallel mechanism has a positive effect on the optimization of mechanical structure and the improvement of mechanical performance. This paper takes a 3-DOF parallel mechanism with kinematic redundancy (PM-KR) as the research object. By building its structure model, the singular position and workspace of the mechanism can be solved. PM-KR can improve the fault tolerance of the mechanism while avoiding singular positions. By changing the height of the redundant component z_p, the workspace of the mechanism can be adjusted, and various singular positions of the mechanism can be avoided, which proves that it is a parallel mechanism with good kinematic performance. The kinematics simulation of the three singular positions of the mechanism is carried out, exploring the impact of changes in the structural parameters of redundant components on the performance of avoiding singular positions, which can prove that this kinematic redundant structure design of the mechanism has obvious advantages.

2 Kinematics Analysis of PM-KR

2.1 Structure Description

The kinematically redundant parallel mechanism studied in this paper is shown in Figure 1. This parallel mechanism consists of a fixed base, an equilateral triangular moving

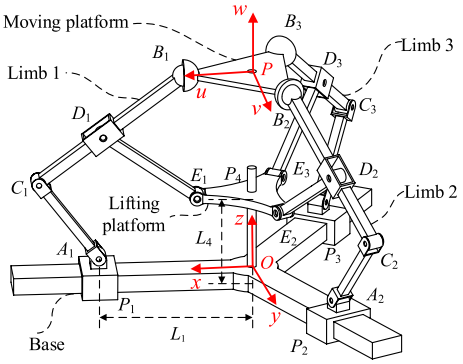

Figure 1 The model of 3-DOF PM-KR

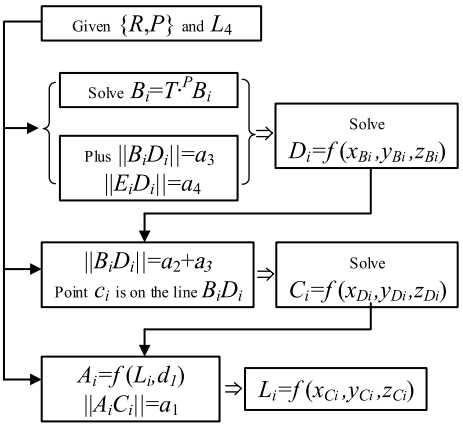

Figure 2 The inverse kinematics solution process of the mechanism

platform, three kinematic limbs with the same structure and a lifting platform. Qu et al. [17] proved that the moving platform has three independent movements, and the mobility of the whole mechanism is equal to 4. The 4 prismatic joints connected to the base are selected as the actuating joints, respectively L_1, L_2, L_3, and L_4.

One side of the limbs of the mechanism is connected to the base by a prismatic joint, and three prismatic joints are all actuating joints. The other side is connected to the moving platform through a spherical joint. The rotation joints of each limb are passive and are parallel to each other. A_i, C_i, D_i and E_i ($i = 1, 2, 3$) are the center points of the rotating joints in each limb; B_i is the center point of the spherical joint in each limb; P_4 is the center point of the lifting platform; the link B_iC_i connects to the link D_iE_i and passes through the rotating joint D_i, and D_i is a point of the link B_iC_i. Links A_iC_i, D_iE_i, and B_iC_i are denoted as link l_{i1}, link l_{i2}, and link l_{i3} ($i = 1, 2, 3$), respectively. The coordinate systems O-xyz and P-uvw are establish. The z-axis is perpendicular to the base; the x-axis is towards the actuating joint P_1; the w-axis is perpendicular to the moving platform, and the u-axis is towards the joint B_1.

2.2 Inverse Kinematics Solution

The detailed process to solve the inverse kinematics solution of the mechanism is shown in Figure 2.

As shown in Figure 3, it is the geometric structure of the mechanism. The base coordinate system $\{O\}$ is O-xyz with the y-axis pointing out of the paper and x-axis aligned with the axis of prismatic joint P_i. The moving platform coordinate system $\{P\}$ is P-uvw with the w-axis perpendicular to the u-axis and the v-axis.

The position of the center point P of the moving platform can be defined as shown in Eq. (1).

$$^{O}\boldsymbol{P} = \begin{bmatrix} x_p & y_p & z_p \end{bmatrix}^{\mathrm{T}}, \tag{1}$$

Besides, the rotation matrix $^{O}\boldsymbol{R}_P$ is used to define the position of the moving platform relative to the base coordinate system $\{O\}$, using the expression of pitch-roll-yaw, as shown in Eqs. (2) and (3).

$$^{O}\boldsymbol{R}_P = \begin{bmatrix} u_x & v_x & w_x \\ u_y & v_y & w_y \\ u_z & v_z & w_z \end{bmatrix}, \tag{2}$$

$$^{O}\boldsymbol{R}_P = \boldsymbol{R}_z(\gamma)\boldsymbol{R}_y(\beta)\boldsymbol{R}_x(\alpha) = \begin{bmatrix} c\beta c\gamma & c\gamma s\alpha s\beta - c\alpha s\gamma & c\alpha c\gamma s\beta + s\alpha s\gamma \\ c\beta s\gamma & s\alpha s\beta s\gamma + c\alpha c\gamma & c\alpha s\beta s\gamma - c\gamma s\alpha \\ -s\beta & c\beta s\alpha & c\alpha c\beta \end{bmatrix}, \tag{3}$$

where, α, β and γ are respectively expressed as Euler angles of the moving platform about the x, y and z axes. Therefore, according to Eq. (4), the midpoint's representation on the moving platform in $\{O\}$ can be obtained.

$$^{O}P = {}^{O}\boldsymbol{R}_P{}^{P}\boldsymbol{P} + \boldsymbol{OP}. \tag{4}$$

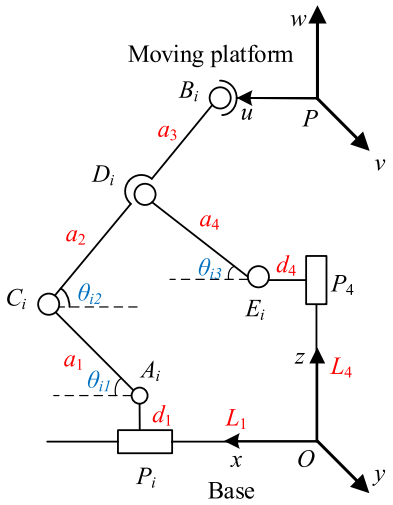

Figure 3 The geometric structure of the mechanism

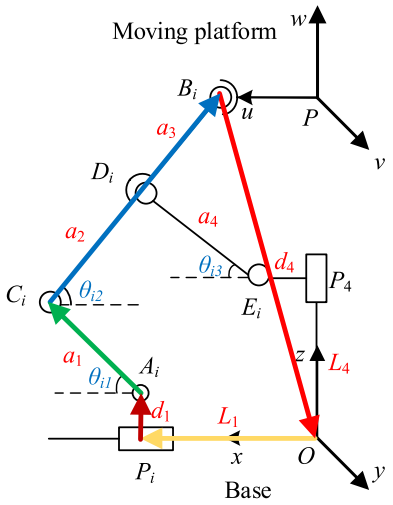

Figure 4 Diagram of closed-loop 1

The positions of the three spherical joints in the moving platform coordinate system $\{B\}$ are expressed in Eq. (5).

$$\begin{cases} {}^{P}\boldsymbol{B}_1 = \begin{bmatrix} r & 0 & 0 \end{bmatrix}^{\mathrm{T}}, \\ {}^{P}\boldsymbol{B}_2 = \begin{bmatrix} -r/2 & \sqrt{3}r/2 & 0 \end{bmatrix}^{\mathrm{T}}, \\ {}^{P}\boldsymbol{B}_3 = \begin{bmatrix} -r/2 & -\sqrt{3}r/2 & 0 \end{bmatrix}^{\mathrm{T}}. \end{cases} \tag{5}$$

According to Eq. (5), the transformation formula of the three spherical joints can be obtained, as shown in Eq. (6).

$${}^{O}\boldsymbol{B}_i = {}^{O}R_P\,{}^{P}\boldsymbol{B}_i + \boldsymbol{OP}. \tag{6}$$

Through calculation, the basic coordinate vector representation of $\boldsymbol{B}_i$ $(i = 1,2,3)$ can be obtained, as shown in Eqs. (7–9).

$${}^{O}\boldsymbol{B}_1 = \begin{bmatrix} x_p + ru_x \\ y_p + ru_y \\ z_p + ru_z \end{bmatrix} = \begin{bmatrix} x_p + r\cos\beta\cos\gamma \\ y_p + r\cos\beta\sin\gamma \\ z_p - r\sin\beta \end{bmatrix}, \tag{7}$$

$${}^{O}\boldsymbol{B}_2 = \begin{bmatrix} x_p - \frac{1}{2}r\left(\cos\beta\cos\gamma + \sqrt{3}(-\cos\gamma\sin\alpha\sin\beta + \cos\alpha\sin\gamma)\right) \\ y_p - \frac{1}{2}r\cos\beta\sin\gamma + \frac{\sqrt{3}}{2}r(\cos\alpha\cos\gamma + \sin\alpha\sin\beta\sin\gamma) \\ z_p + \frac{1}{2}r(\sqrt{3}\cos\beta\sin\alpha + \sin\beta) \end{bmatrix}, \tag{8}$$

$${}^{O}\boldsymbol{B}_3 = \begin{bmatrix} x_p + \frac{1}{2}r\left(-\cos\beta\cos\gamma + \sqrt{3}(-\cos\gamma\sin\alpha\sin\beta + \cos\alpha\sin\gamma)\right) \\ y_p - \frac{1}{2}r\left(\sqrt{3}\cos\alpha\cos\gamma + (\cos\beta + \sqrt{3}\sin\alpha\sin\beta\sin\gamma)\right) \\ z_p + \frac{1}{2}r(-\sqrt{3}\cos\beta\sin\alpha + \sin\beta) \end{bmatrix}. \tag{9}$$

The base coordinate vector representation of the point $\boldsymbol{A}_i$ $(i = 1,2,3)$ is shown in Eq. (10).

$$\begin{cases} {}^{O}\boldsymbol{A}_1 = \begin{bmatrix} L_1 & 0 & d_1 \end{bmatrix}^{\mathrm{T}}, \\ {}^{O}\boldsymbol{A}_2 = \begin{bmatrix} -1/2L_2 & \sqrt{3}/2L_2 & d_1 \end{bmatrix}^{\mathrm{T}}, \\ {}^{O}\boldsymbol{A}_3 = \begin{bmatrix} -1/2L_3 & -\sqrt{3}/2L_3 & d_1 \end{bmatrix}^{\mathrm{T}}. \end{cases} \tag{10}$$

According to the position coordinates of $\boldsymbol{A}_i$ and $\boldsymbol{B}_i$, the distance between the joint A_i and the joint B_i can be calculated, as shown in Eq. (11).

$$\boldsymbol{A}_i\boldsymbol{B}_i = \boldsymbol{B}_i - \boldsymbol{A}_i. \tag{11}$$

The vector $\boldsymbol{s}_i$ is set in three directions on the base, as shown in Eq. (12).

$$\begin{cases} {}^{O}\boldsymbol{s}_1 = \begin{bmatrix} 0 & 1 & 0 \end{bmatrix}^{\mathrm{T}}, \\ {}^{O}\boldsymbol{s}_2 = \begin{bmatrix} \sqrt{3} & 1 & 0 \end{bmatrix}^{\mathrm{T}}, \\ {}^{O}\boldsymbol{s}_3 = \begin{bmatrix} -\sqrt{3} & 1 & 0 \end{bmatrix}^{\mathrm{T}}. \end{cases} \tag{12}$$

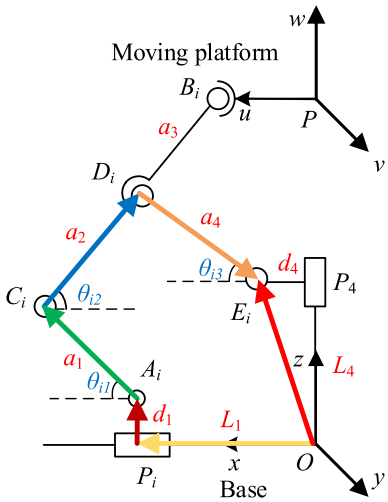

Figure 5 Diagram of closed-loop 2

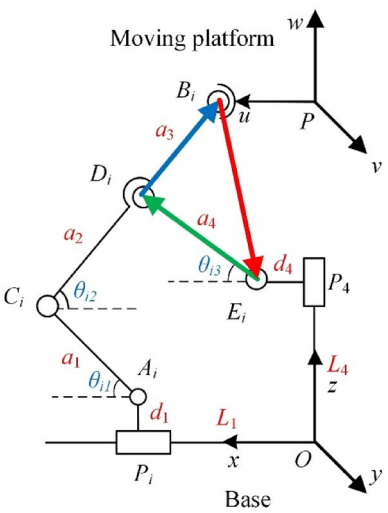

Figure 6 Diagram of closed-loop 3

Because $\boldsymbol{s}_i$ is perpendicular to $\boldsymbol{A}_i\boldsymbol{B}_i$, the dot product of the two vectors is equal to 0, and the expressions of x_p, y_p, and γ can be obtained, as shown in Eqs. (13)–(15).

$$x_p = -\frac{r\left(\cos^2\alpha - \cos^2\beta + \sin^2\alpha\sin^2\beta\right)}{2\sqrt{(1+\cos\alpha\cos\beta)^2}}, \tag{13}$$

$$y_p = -\frac{r\cos\beta\sin\alpha\sin\beta}{\sqrt{(1+\cos\alpha\cos\beta)^2}}, \tag{14}$$

$$\gamma = \arctan\left[\frac{\cos\alpha+\cos\beta}{\sqrt{(1+\cos\alpha\cos\beta)^2}}, \frac{\sin\alpha\sin\beta}{\sqrt{(1+\cos\alpha\cos\beta)^2}}\right]. \tag{15}$$

According to the above method, the coordinate representation of the remaining joints on the limb can be obtained sequentially.

The inverse solution of the mechanism is that the parameters α, β and z_p of the moving platform are known, and the actuating lengths L_1, L_2 and L_3 of the input prismatic joints are calculated. According to the vector closed-loop principle, a vector closed-loop equation is established in a limb of this mechanism, as shown in Figure 4. The four vector combinations $\boldsymbol{OA}_1$, $\boldsymbol{A}_1\boldsymbol{C}_1$, $\boldsymbol{C}_1\boldsymbol{B}_1$, $\boldsymbol{B}_1\boldsymbol{O}$ are selected as the closed-loop.

According to Figure 4, the closed-loop equation 1 of limb 1 can be obtained, as shown in Eq. (16).

$$\boldsymbol{OP}_1 + \boldsymbol{P}_1\boldsymbol{A}_1 + \boldsymbol{A}_1\boldsymbol{C}_1 + \boldsymbol{C}_1\boldsymbol{B}_1 = \boldsymbol{OB}_1. \tag{16}$$

Then Eq. (16) is expressed with the structural parameters of the mechanism, as shown in Eq. (17).

$$\begin{bmatrix} x_{a1} \\ 0 \\ z_{a1} \end{bmatrix} + \begin{bmatrix} a_1\cos\theta_{11} \\ 0 \\ a_1\sin\theta_{11} \end{bmatrix} + \begin{bmatrix} -(a_2+a_3)\cos\theta_{12} \\ 0 \\ (a_2+a_3)\sin\theta_{12} \end{bmatrix} = \begin{bmatrix} x_{b1} \\ 0 \\ z_{b1} \end{bmatrix}. \tag{17}$$

Because the mechanism is a parallel mechanism with kinematic redundancy, its redundant structure is a lifting platform. The two closed-loop equations of the limb are solved simultaneously, as shown in Figures 5 and 6.

According to Figure 5, the closed-loop equation 2 of limb 1 can be obtained as Eq. (18).

$$\boldsymbol{OP}_1 + \boldsymbol{P}_1\boldsymbol{A}_1 + \boldsymbol{A}_1\boldsymbol{C}_1 + \boldsymbol{C}_1\boldsymbol{D}_1 + \boldsymbol{D}_1\boldsymbol{E}_1 = \boldsymbol{OE}_1. \tag{18}$$

Then Eq. (18) is expressed with the structural parameters of the mechanism, as shown in Eq. (19).

$$\begin{bmatrix} x_{a1} \\ 0 \\ z_{a1} \end{bmatrix} + \begin{bmatrix} a_1\cos\theta_{11} \\ 0 \\ a_1\sin\theta_{11} \end{bmatrix} + \begin{bmatrix} -a_2\cos\theta_{12} \\ 0 \\ a_2\sin\theta_{12} \end{bmatrix} + \begin{bmatrix} -a_4\cos\theta_{13} \\ 0 \\ -a_4\sin\theta_{13} \end{bmatrix} = \begin{bmatrix} x_{e1} \\ 0 \\ z_{e1} \end{bmatrix}. \tag{19}$$

As shown in Figure 6, the closed-loop equation 3 of limb 1 can be obtained, as shown in Eq. (20).

$$\boldsymbol{E}_1\boldsymbol{D}_1 + \boldsymbol{D}_1\boldsymbol{B}_1 = \boldsymbol{E}_1\boldsymbol{B}_1. \tag{20}$$

Then Eq. (20) is expressed with the structural parameters of the mechanism, as shown in Eq. (21).

$$\begin{bmatrix} a_4\cos\theta_{13} \\ 0 \\ a_4\sin\theta_{13} \end{bmatrix} + \begin{bmatrix} -a_3\cos\theta_{12} \\ 0 \\ a_3\sin\theta_{12} \end{bmatrix} = \begin{bmatrix} x_{b1} - x_{e1} \\ 0 \\ z_{b1} - z_{e1} \end{bmatrix}. \tag{21}$$

Eqs. (16)–(21) are expanded to get six equations, as shown in Eq. (22).

$$\begin{cases} x_{a1} + a_1\cos\theta_{11} - (a_2 + a_3)\cos\theta_{12} = x_{b1}, \\ z_{a1} + a_1\sin\theta_{11} + (a_2 + a_3)\sin\theta_{12} = z_{b1}, \\ x_{a1} + a_1\cos\theta_{11} - a_2\cos\theta_{12} - a_4\cos\theta_{13} = x_{e1}, \\ z_{a1} + a_1\sin\theta_{11} + a_2\sin\theta_{12} - a_4\sin\theta_{13} = z_{e1}, \\ a_4\cos\theta_{13} - a_3\cos\theta_{12} = x_{b1} - x_{e1}, \\ a_4\sin\theta_{13} + a_3\sin\theta_{12} = z_{b1} - z_{e1}. \end{cases} \tag{22}$$

According to the coordinate expressions of B_1 and E_1, D_1 is taken as the center of the circle, B_1D_1, and E_1D_1 as the radius. The equations of the two circles are listed respectively, and the coordinates of D_1 can be solved, as shown in the Eqs. (23) and (24).

$$(x_{d1} - x_{b1})^2 + (z_{d1} - z_{b1})^2 = a_3^2, \tag{23}$$

$$(x_{d1} - x_{e1})^2 + (z_{d1} - z_{e1})^2 = a_4^2. \tag{24}$$

According to the coordinates of B_1 and D_1 and the tangent formula of the triangle, the size of θ_{13} can be solved, as shown in Eq. (25).

$$\theta_{13} = \arctan\frac{z_{d1} - z_{e1}}{x_{d1} - x_{e1}}. \tag{25}$$

According to the closed-loop equation (22), the size of θ_{12} can be solved, as shown in Eq. (26).

$$\theta_{12} = \arccos\frac{-x_{b1} + x_{e1} + a_4\cos\theta_{13}}{a_3}. \tag{26}$$

Simultaneously eliminating θ_{12} in Eqs. (22) and (27) can be obtained.

$$a_1^2 + (x_{a1} - x_{b1})^2 + 2a_1(x_{a1} - x_{b1})\cos\theta_{11} + (z_{a1} - z_{b1})^2 + 2a_1(z_{a1} - z_{b1})\sin\theta_{11} = (a_2 + a_3)^2. \tag{27}$$

According to Eq. (27), the expression of θ_{11} can be obtained, as shown in Eq. (28).

$$\theta_{11} = \arctan\left(\frac{-a_1(x_{a1} - x_{b1})\left(a_1^2 - (a_2 + a_3)^2 + (x_{a1} - x_{b1})^2 + (z_{a1} - z_{b1})^2\right)}{a_1^2\left((x_{a1} - x_{b1})^2 + (z_{a1} - z_{b1})^2\right)} + \frac{\sqrt{-a_1^2\left(-a_1 + a_2 + a_3)^2 - (x_{a1} - x_{b1})^2 - (z_{a1} - z_{b1})^2\right)}}{a_1^2\left((x_{a1} - x_{b1})^2 + (z_{a1} - z_{b1})^2\right)} \frac{\sqrt{\left((a_1 + a_2 + a_3)^2 - (x_{a1} - x_{b1})^2 - (z_{a1} - z_{b1})^2\right)(z_{a1} - z_{b1})^2}}{a_1^2\left((x_{a1} - x_{b1})^2 + (z_{a1} - z_{b1})^2\right)}\right). \tag{28}$$

According to Eq. (22), only the actuating parameter L_1 is unknown in the equation. By solving the equation, the expression equation of L_1 can be obtained, as shown in Eq. (29).

$$L_1 = x_{e1} - a_1\cos\theta_{11} - a_2\cos\theta_{12} - a_4\cos\theta_{13}. \tag{29}$$

In the same way, the expressions for actuating lengths L_2 and L_3 can be obtained by the closed-loop equations of limb 2 and limb 3, as shown in Eqs. (30) and (31).

$$L_2 = -2x_{e2} - a_1\cos\theta_{21} + a_2\cos\theta_{22} + a_4\cos\theta_{23}, \tag{30}$$

$$L_3 = -2x_{e3} - a_1\cos\theta_{31} + a_2\cos\theta_{32} + a_4\cos\theta_{33}. \tag{31}$$

2.3 Singularity Analysis

The positive Jacobian matrix $\boldsymbol{J}_q$ is the relationship between the twist $\boldsymbol{\chi}$ of the motion platform expressed by the six-dimensional vector and the rate of changing $\boldsymbol{L}_i$ of the actuating length, as shown in Eq. (32).

$$\boldsymbol{L}_i = \boldsymbol{J}_q\boldsymbol{\chi}. \tag{32}$$

The Jacobian matrix of the parallel mechanism with kinematic redundancy is the relationship between the angular velocity $\boldsymbol{\omega}$ of the moving platform and the vector $\boldsymbol{L}_1$, $\boldsymbol{L}_2$, and $\boldsymbol{L}_3$ of the actuating joint change rate, as shown in Eq. (33).

$$\boldsymbol{L} = \boldsymbol{J}\cdot\boldsymbol{\omega}. \tag{33}$$

The relationship among the inverse Jacobian matrix $\boldsymbol{J}_x$, the three-dimensional twist vector $\boldsymbol{\chi}$ of the moving platform, and the angular velocity $\boldsymbol{\omega}$ is shown in Eq. (34).

$$\boldsymbol{\chi} = \begin{bmatrix} {}^A\boldsymbol{v}_p \\ \boldsymbol{\omega} \end{bmatrix} = \boldsymbol{J}_x\boldsymbol{\omega}. \tag{34}$$

where $\boldsymbol{\chi}$ represents the moving platform's twist; ${}^A\boldsymbol{v}_p$ is the speed of the moving platform, and $\boldsymbol{\omega}$ is the angular velocity of the moving platform.

The closed-loop 2 of the limb1, 2, 3 is selected. According to the result of the inverse solution, the constraint equations of limbs 1, 2, and 3 are shown in Eqs. (35)–(37).

$$\begin{aligned}&(x_{a1} - x_{e1} - a_2\times\cos\theta_{12} - a_4\cos\theta_{13})^2 \\ &+ (z_{a1} - z_{e1} + a_2\sin\theta_{12} - a_4\sin\theta_{13})^2 = a_1^2,\end{aligned} \tag{35}$$

$$\begin{aligned}&(2x_{a2} - 2x_{e2} - a_2\cos\theta_{22} + a_4\cos\theta_{23})^2 \\ &+ (z_{a2} - z_{e2} + a_2\sin\theta_{22} - a_4\sin\theta_{23})^2 = a_1^2,\end{aligned} \tag{36}$$

$$\begin{aligned}&(2x_{a3} - 2x_{e3} + a_2\cos\theta_{32} + a_4\cos\theta_{33})^2 \\ &+ (z_{a3} - z_{e3} + a_2\sin\theta_{32} - a_4\sin\theta_{33})^2 = a_1^2.\end{aligned} \tag{37}$$

The partial derivative of the time t is calculated in the actuating parameters L_1, L_2, L_3, and the moving platform motion parameters α, β, z_p. After simplification, the Eqs. (38)–(40) can be obtained.

$$e_1 = e_{11}\times\dot{\alpha} + e_{12}\times\dot{\beta} + e_{13}\times\dot{z}_p + e_{14}\times\dot{L}_1, \tag{38}$$

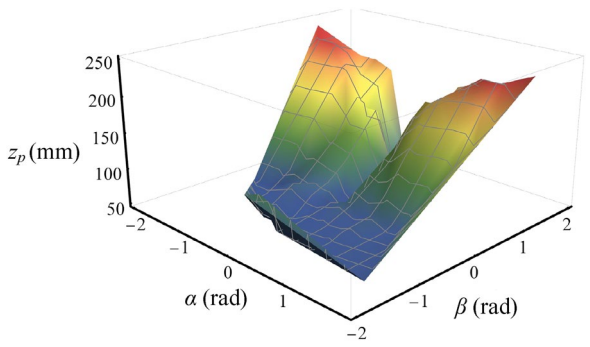

Figure 7 Singular diagram of mechanism when $L_4 = 80$ mm

$$e_2 = e_{21}\times\dot{\alpha} + e_{22}\times\dot{\beta} + e_{23}\times\dot{z}_p + e_{24}\times\dot{L}_2, \tag{39}$$

$$e_3 = e_{31}\times\dot{\alpha} + e_{32}\times\dot{\beta} + e_{33}\times\dot{z}_p + e_{34}\times\dot{L}_3. \tag{40}$$

In Eqs. (38)–(40), e_{ij} (i = 1,2,3 and j = 1,2,3,4) respectively represent the result of the combination of the same type and the simplified expressions of the result in Eqs. (35)–(37). Because these expressions are too long, they are not shown in the paper.

Extracting the common parameter items in the above equations, the positive Jacobian matrix $\boldsymbol{J}_q$ and the inverse Jacobian matrix $\boldsymbol{J}_x$ can be obtained as Eqs. (41) and (42).

$$\boldsymbol{J}_q = \begin{bmatrix} e_{14} & 0 & 0 \\ 0 & e_{24} & 0 \\ 0 & 0 & e_{34} \end{bmatrix}, \tag{41}$$

$$\boldsymbol{J}_x = \begin{bmatrix} e_{11} & e_{12} & e_{13} \\ e_{21} & e_{22} & e_{23} \\ e_{31} & e_{32} & e_{33} \end{bmatrix}. \tag{42}$$

The singularity of the mechanism is solved. The structural parameters of the mechanism are set, d_1 = 30 mm, a_1 = 114 mm, a_2 = 92 mm, a_3 = 115 mm, a_4 = 132 mm, d_4 = 62.68 mm, r = 78 mm. The range of z_p is set as [150, 210] mm, and the range of α and β is set as [−2, 2] rad.

Let $Det(\boldsymbol{J}_x) = 0$, the actuating parameter L_4 is taken as the structure parameter of the mechanism. When L_4 = 80 mm, the height of the lifting platform is located between the base and the moving platform, so that the mechanism as a whole maintains a normal working state. When the actuating joint changes, the height of the lifting platform will not have a significant impact on the position and posture of the mechanism. And

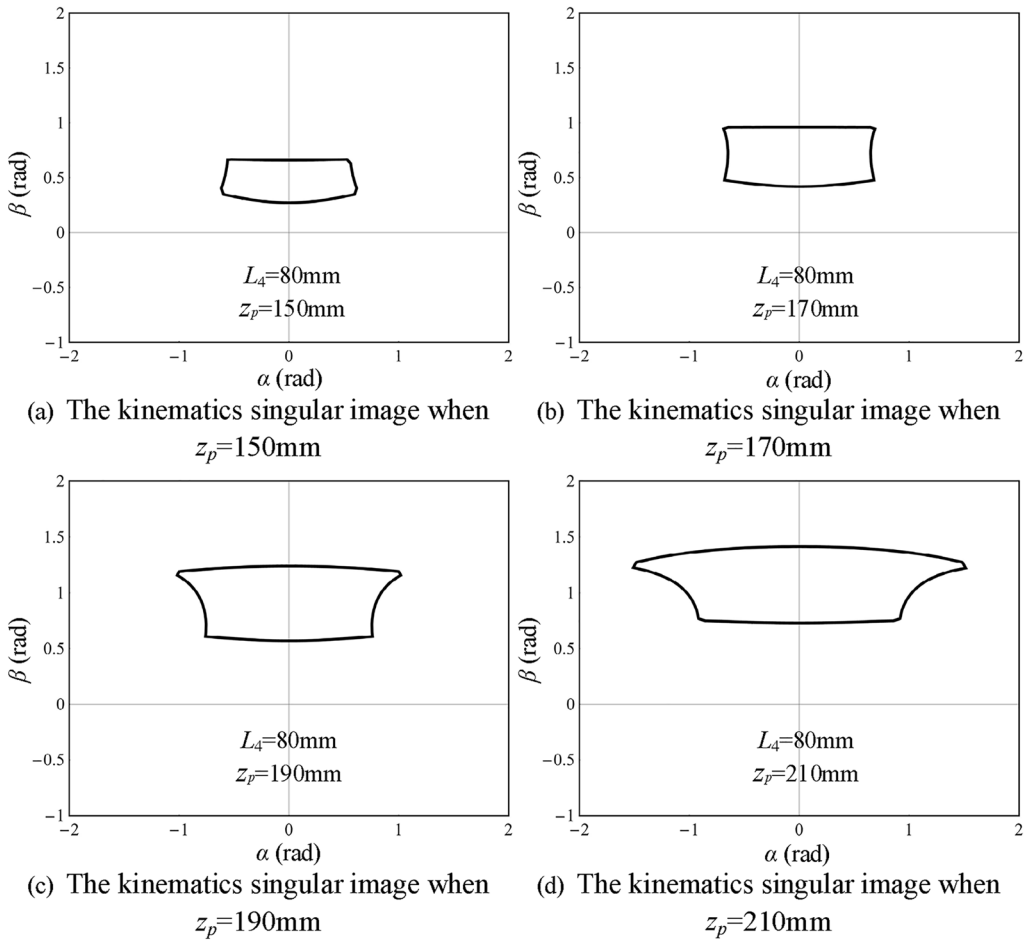

Figure 8 The singularity diagram of the mechanism when z_p takes different values

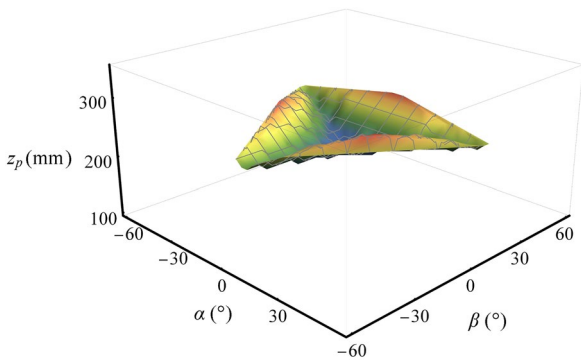

Figure 9 Three-dimensional curve diagram of the workspace

the singularity diagram of the mechanism under L_4 = 80 mm is measured, as shown in Figure 7.

Set z_p = 150/170/190/ 210 mm, respectively, and the positive motion singular images of the mechanism under different values of z_p are measured, as shown in Figure 8.

By analyzing the Jacobian matrix and singular image of the mechanism, the singular position of the mechanism can be obtained [31–33]. When $\theta_{i1} = \pi/2$ and $\theta_{i2} = 0°$of a limb, the mechanism will have a singular position 1, as shown in Figure 20a. When $\theta_{i1} = \theta_{i2} = \pi/2$ of the three limbs, the mechanism will have a singular position 2, as shown in Figure 24a. When $\theta_{i1} = 0°$ of a limb, the mechanism produces a singular position 3, as shown in Figure 26a. The redundant components of the mechanism called lifting platform, its position will affect the singularity of the mechanism, which will be analyzed in the content.

2.4 Workspace Analysis

The structural parameters of the mechanism are set, $d_1 = 30$ mm, $a_1 = 114$ mm, $a_2 = 92$ mm, $a_3 = 115$ mm, $a_4 = 132$ mm, $d_4 = 62.68$ mm, $r = 78$ mm.

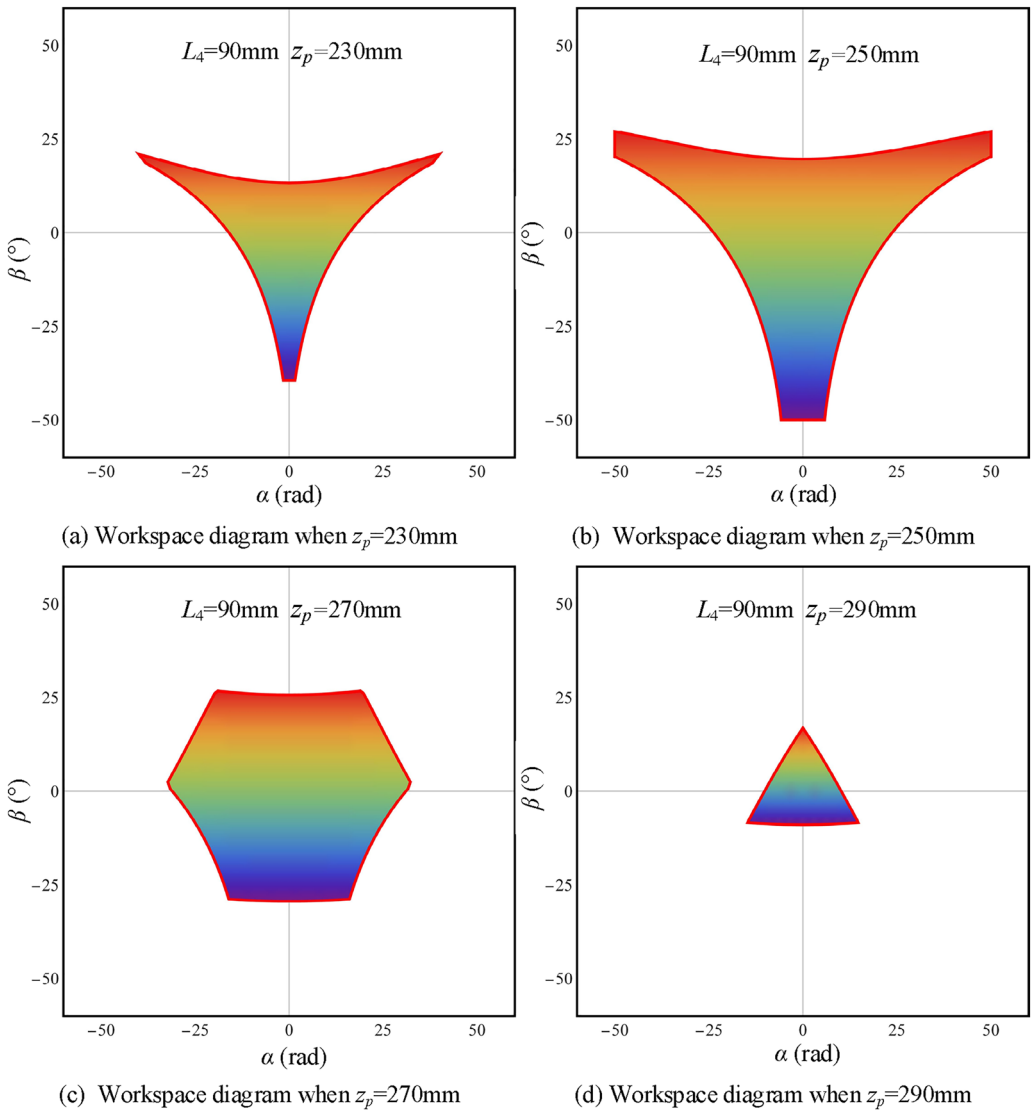

(a) Workspace diagram when z_p=230mm (b) Workspace diagram when z_p=250mm

(c) Workspace diagram when z_p=270mm (d) Workspace diagram when z_p=290mm

Figure 10 Workspace of mechanism with different values of z_p

The workspace of the mechanism is analyzed by adopting the workspace search method. The length of the actuating joint L_4 is set as a fixed value, and the point set is obtained where the workspace satisfies the inverse solution of the mechanism. Finally, we can get the workspace diagram of the mechanism.

Analyzing limb 1, according to the Eqs. (25)–(28) of θ_{11}, θ_{12}, θ_{13} obtained by the inverse solution, substituting the above three equations into Eq. (29), we can get L_1's expression only have the moving platform kinematic parameters include α, β, and z_p. Similarly, we can get L_1, and L_2's expression only has the moving platform kinematic parameters including α, β, and z_p.

The value range of L_1, L_2, and L_3 is set as [50, 200] mm; the range of z_p is set as [50, 350] mm, and the value range of α and β is set to $[-\pi/2, \pi/2]$. L_4 is used as a structural

Table 1 Changes of kinematic parameters α and β of the moving platform

z_p (mm)	α (°)	β (°)
210	[− 40, 40]	[− 42, 24]
230	[− 46, 46]	[− 48, 28]
250	[− 66, 66]	[− 66, 34]
270	[− 52, 52]	[− 50, 34]
290	[− 40, 40]	[− 32, 36]
310	[− 28, 28]	[− 16, 32]

parameter, and the workspace of the mechanism can be calculated when $L_4 = 90$ mm.

The surface image [34] of the workspace of the analyzed mechanism can be obtained, as shown in Figure 9, by using the method of fitting a surface with a set of points and fitting the workspace point set of the mechanism.

Based on the obtained workspace in Figure 9, the workspace diagram of the mechanism with $z_p = 230/250/270/290$ mm can be sketched, as shown in Figure 10. The moving platform parameters α and β are variables, and z_p is a fixed value.

By analyzing the workspace of the mechanism, we can get the changes of the moving platform kinematics parameters α and β when the moving platform parameter z_p is a fixed value, as shown in Table 1.

Table 1 shows that when the moving platform is in working condition, the maximum angle α and β of its rotation around the x and y axes can reach 66°. The moving platform of this mechanism has the characteristics of a large rotation angle compared with the general parallel mechanism, which can meet the needs of specific working conditions.

3 The Influence of Redundant Components on Mechanism's Kinematics

Adding a redundant part to a general parallel mechanism, the kinematic characteristics of the mechanism will be affected, such as fault tolerance, workspace, and singularity [35]. This section researches the impact of redundant components, analyzing the influence of the change of redundant part's parameters on the mechanism's kinematics.

3.1 Analysis of Mechanism Fault Tolerance

Fault tolerance refers to the change in the mechanism's kinematic performance when a part of the mechanism fails. The better the fault-tolerant mechanism is, the smaller the difference in the mechanism's kinematics when the components fail. For the mechanism with poor fault-tolerant performance, the components' failure will significantly impact the overall kinematics of the mechanism.

When one of the actuating joints of the parallel mechanism fails, the overall kinematic performance of the mechanism will be affected. Compared with the normal mechanism, the DOF of the mechanism with failed actuating joints will be less or even zero, and the mechanism will not have any kinematic performance. A parallel mechanism with good kinematics has better fault tolerance, that is, when multiple actuating joints fail, it still has certain kinematic performance.

There are many indexes for measuring the fault tolerance performance of a mechanism, such as changes in the workspace, changes in actuating torque, and each joint's integrity. In measuring the fault-tolerant performance of the 3-DOF PM-KR, the change of the workspace is selected as the performance index. When a specific actuating joint of the mechanism fails, the influence on the mechanism's workspace will be very obvious. As a result, the change of the workspace of the mechanism is used to test the fault tolerance performance of the mechanism.

As shown in Figure 11, the image of the workspace of the mechanism when the machine is operating normally, the actuating joint P_1 fails, the actuating joints P_1 and P_2 all fail. In the image, the moving platform kinematic parameters $z_p = 210–310$ mm, the height of the lifting platform $L_4 = 90$ mm, the kinematics parameters of the moving platform α, $\beta \in [-90°, 90°]$, the actuating parameters $L_1, L_2, L_3 \in [50, 200]$ mm.

The point search method is adopted to analyze the fault-tolerant performance of the mechanism, and the distance between the points is 3 mm. First, on the condition that the mechanism is normal, the number of points in the workspace is used as the base. Then the effective proportion of the workspace is analyzed when one actuating joint fails and when two actuating joints fail simultaneously.

As shown in Table 2, it can be found that when the kinematic parameters of the moving platform $z_p = 210/230/250/310$ mm, the workspace when the actuating joint P_1 fails is about 60% of the normal workspace. When the actuating joint P_1 and P_2 fail simultaneously, the workspace is about 30% of the normal workspace, indicating that the mechanism has better performance in this moving platform height.

When the moving platform's kinematic parameters are $z_p = 270/290$ mm, the workspace when the actuating joint P_1 fails is about 30% of the normal workspace. When the actuating joint P_1 and P_2 fail simultaneously, the workspace is about 10% of the normal workspace. Compared with the fault tolerance of the mechanism obtained by the previous parameters, the mechanism's fault tolerance performance decreases.

Moreover, the position where the actuating joint fails has an impact on the fault tolerance of the mechanism. Measure the influence of the position where the actuating joint fails on the workspace. When the actuating joint P_1 fails, P_1 and P_2 fail simultaneously, the influence of the failure position of the actuating joint on the workspace is shown in Table 3.

Through the analysis of Table 3, we can find that when the actuating joint fails at [50, 100] mm, the workspace when the actuating joint P_1 fails is 10.91% of the normal workspace, and the workspace when the actuating joints P_1 and P_2 fail simultaneously is 1.9% of the normal workspace. Because this position of the actuating joint is very

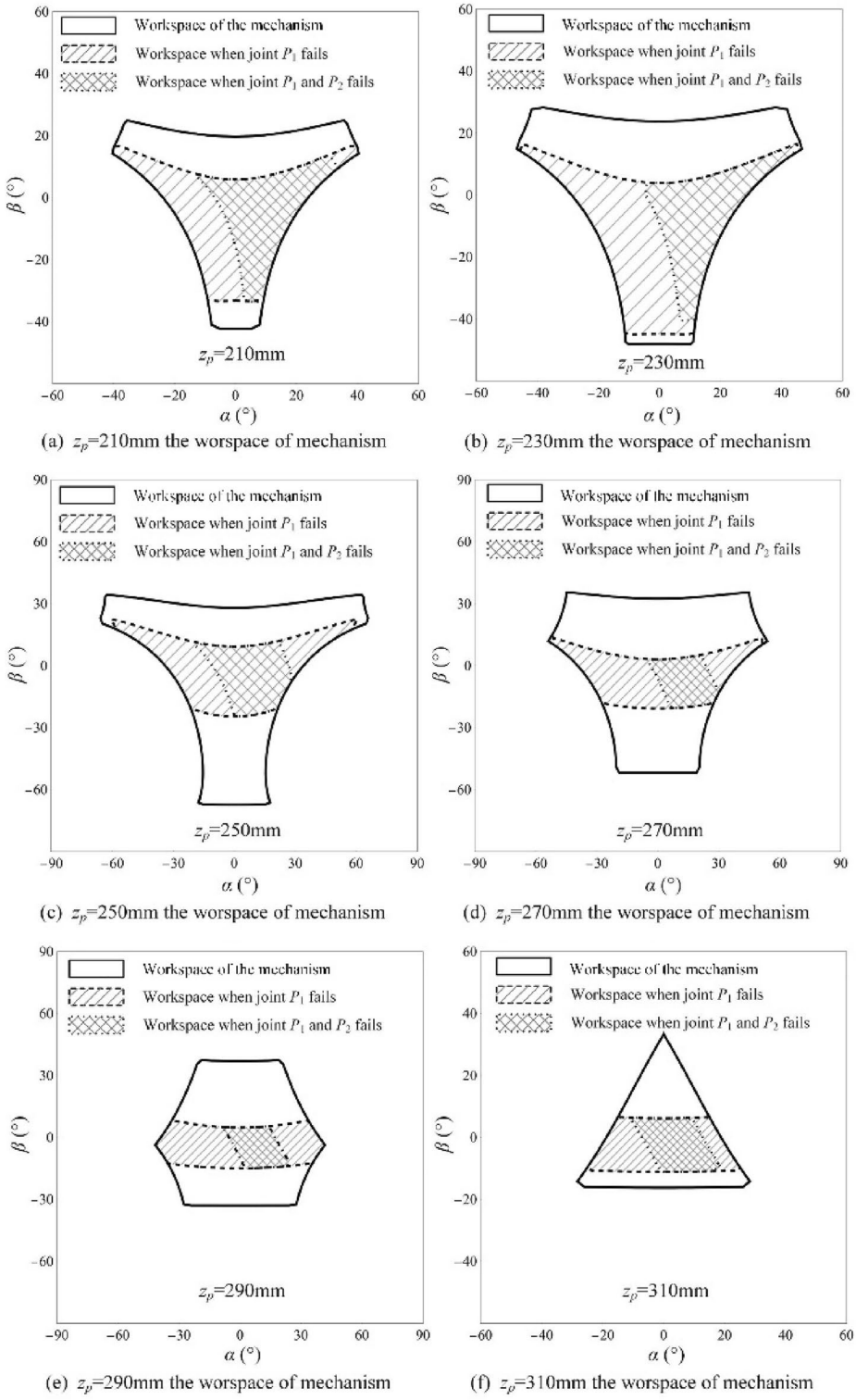

(a) z_p=210mm the worspace of mechanism (b) z_p=230mm the worspace of mechanism

(c) z_p=250mm the worspace of mechanism (d) z_p=270mm the worspace of mechanism

(e) z_p=290mm the worspace of mechanism (f) z_p=310mm the worspace of mechanism

Figure 11 Images of the workspace when the $L_4 = 90$ mm

Table 2 Changes in the workspace of the mechanism

z_p (mm)	All points in the workspace	Number of workspace points when P_1 fails	Number of workspace points when P_1 and P_2 fail simultaneously
210	102	62 (60.78%)	33 (32.35%)
230	144	81 (56.25%)	34 (23.61%)
250	239	96 (60.78%)	42 (32.35%)
270	237	73 (30.80%)	23 (9.70%)
290	174	59 (33.90%)	16 (9.19%)
310	60	34 (56.67%)	16 (26.67%)

Table 3 The influence of the failure position of the actuating joint on the workspace

The position where the actuating joint fails (mm)	All points in the workspace	Number of workspace points when P_1 fails	Number of workspace points when P_1 and P_2 fail simultaneously
L_i∈[50,100]	4259	465(10.91%)	85(1.9%)
L_i∈[100,150]	4259	1264(29.68%)	505(11.86%)
L_i∈[150,200]	4259	2530(59.40%)	1819(42.71%)

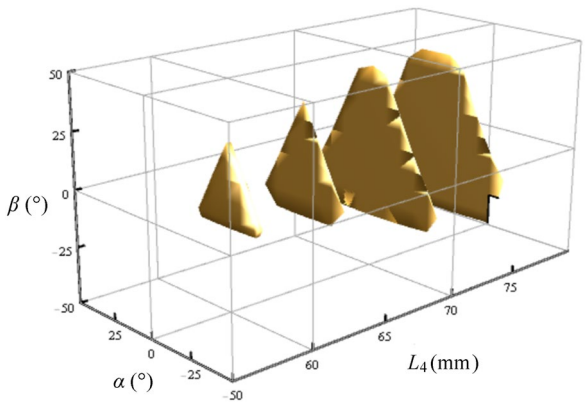

Figure 12 L_4 = 60–75 mm workspace images of the mechanism

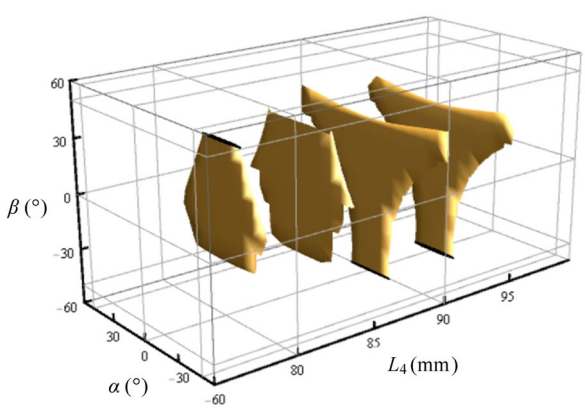

Figure 13 L_4 = 80–95 mm workspace images of the mechanism

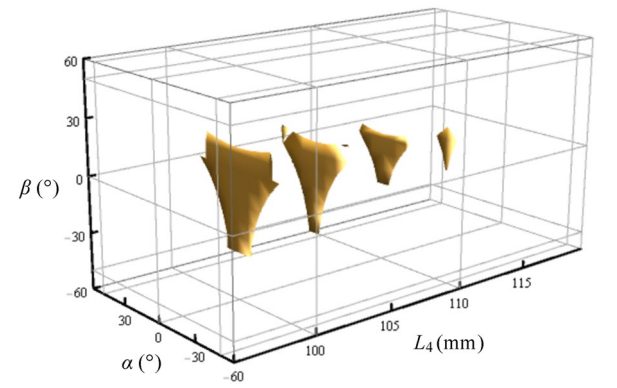

Figure 14 L_4 = 100–115 mm workspace images of the mechanism

close to the center of the whole mechanism, indicating that the actuating joint has a fault at this position, the fault tolerance of the mechanism is very poor. When the fault position of the actuating joint is [100, 150] mm, the fault tolerance of the mechanism is improved, the workspace when the actuating joint P_1 fails is 29.68% of the normal workspace, and the workspace when the actuating joints P_1 and P_2 fail simultaneously is 11.86% of the normal workspace. When the actuating joint's fault position is [150, 200] mm, the fault tolerance of the mechanism is excellent, and the position of the actuating joint is the farthest from the center of the mechanism.

In summary, the 3-DOF PM-KR has good fault tolerance. By analyzing the different height values z_p of the moving platform, the fault tolerance of the mechanism

improves, the maximum workspace when the actuating joint P_1 fails is 60.78% of the normal workspace, and the maximum workspace when the actuating joint P_1 and P_2 fail simultaneously is 32.35% of the normal workspace. At the same time, the position where the actuating joint fails also affects the fault tolerance of the mechanism. When the actuating joint fails farther away from the center, the better the fault tolerance of the mechanism; otherwise, the worse the fault tolerance of the mechanism.

3.2 The Impact of Redundant Components on Workspace

Adding redundant components to the parallel mechanism will have an impact on the entire mechanism's workspace [35, 36]. In the 3-DOF PM-KR, the lifting platform is connected with link l_{i3} through three redundant link l_{i2} ($i = 1, 2, 3$) at rotating joints. The position and posture of each link in the limb change with the height of the lifting platform, which will affect the workspace of the mechanism.

The kinematic parameter $z_p = 250$ mm of the moving platform is set as a fixed value, and the influence of height variation of lifting platform, L_4, on the motion parameters α and β of the moving platform can be obtained. As shown in Figure 12, it is the changing image of the workspace of the mechanism when $L_4 = 60/65/70/75$ mm.

By observing the image of the workspace, it can be concluded that with the increase of the value of L_4, the workspace of the mechanism also becomes larger, indicating that the workspace of the mechanism in this posture increases with the structural parameters of redundant components.

As shown in Figure 13, it is an image of the workspace when $L_4 = 80/85/90/95$ mm. In this posture, when the value of L_4 increases from 80 mm to 90 mm, the workspace continues to increase. But when the value of L_4 continues to increase, the lifting platform is located in the center of the entire mechanism, its position has little influence on the posture of the limb, so the change of the workspace of the mechanism is not apparent.

Continue to increase the value of L_4, and the changing image of the workspace is taken when $L_4 = 100/105/110/115$ mm, as shown in Figure 14. By observing the posture change of the workspace, we can explain that as the value of L_4 increases in this range, the mechanism's workspace is continuously reduced. Since the kinematic parameter z_p of the moving platform is set to a fixed value, in this posture, the lifting platform's height is constantly rising close to the moving platform. At this time, the mechanism's posture

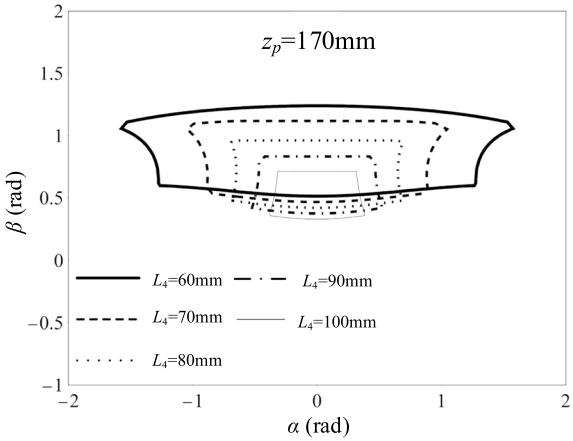

Figure 16 The image of the singular position of the mechanism when $z_p = 170$ mm

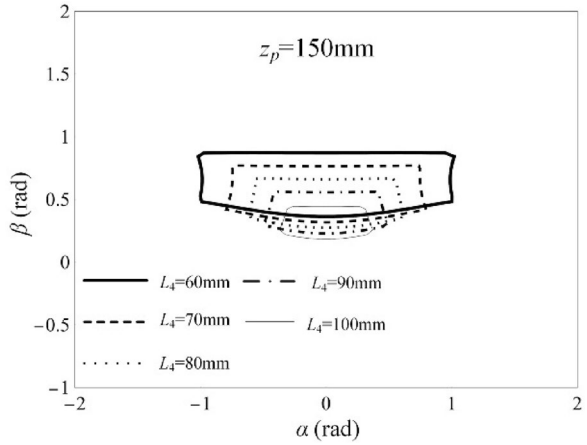

Figure 15 The image of the singular position of the mechanism when $z_p = 150$ mm

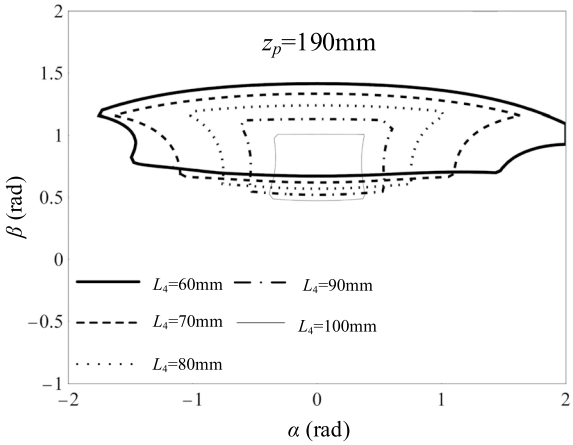

Figure 17 The image of the singular position of the mechanism when $z_p = 190$ mm

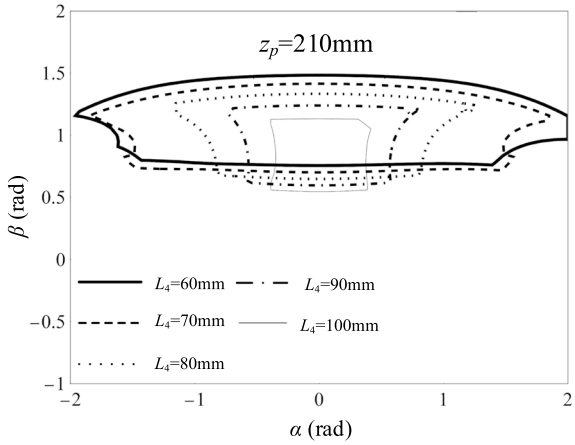

Figure 18 The image of the singular position of the mechanism when $z_p = 210$ mm

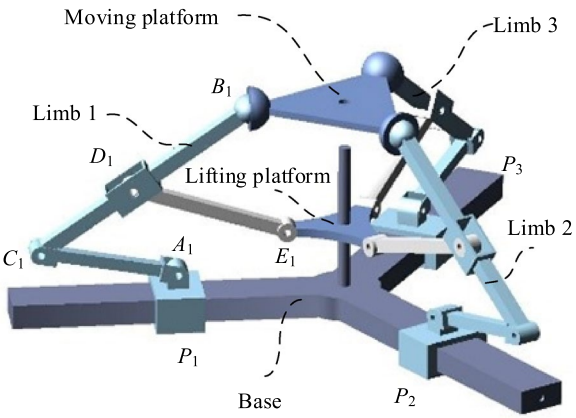

Figure 19 The initial position of the mechanism simulation

inhibits the movement of the limb, which makes the workspace of the mechanism continuously reduced.

Analyzing the mechanism's workspace shows that the change of the kinematic redundant part's position significantly impacts the workspace. When the lifting platform is at the starting position, as its height value increases, the mechanism's workspace also becomes larger. Because each mechanism's workspace is fixed, when the position of the lifting platform reaches a specific height value, the change of the workspace of the mechanism is not obvious at this time. As the lifting platform's height continues to increase, its position slowly approaches the moving platform of the mechanism, and the redundant part has a significant inhibitory effect on the movement of the limb, which causes the workspace to reduce significantly.

3.3 The Effect of Redundant Components on Singularity

The structural parameter's change of the redundant part will impact the mechanism's kinematics, the most significant of which is to change the mechanism to avoid the singularity. Kinematics analysis obtains the Jacobian matrix of the mechanism and then solves the mechanism's singularity. Finally, we can obtain the singular position of the motion posture of the mechanism. In this section, the kinematics parameter z_p of the moving platform changes with the values of the redundant part L_4, and different L_4 corresponds to different singular configurations of the mechanism. Therefore, the influence of the redundant components on the singularity avoidance of the mechanism is analyzed.

As shown in Figure 15, it is an image of the singularity of the mechanism when the moving platform's kinematics parameter is $z_p = 150$ mm. When the value of L_4 is increased from 60 to 100 mm, the singular position's image is significantly reduced. Indicating that at this position, as the lifting platform's height value increases, the point set of the singular position of the mechanism continues to shrink.

When the value of actuating joint L_4 becomes larger, the change of the singular position's range of the mechanism is observed. As shown in Figure 16, it is a singular image when the kinematics parameter z_p of the moving platform of the mechanism is 170 mm, and the value range of L_4 is [60,100] mm. Compared with the singular images, when the height of the moving platform z_p is equal to 150 mm, the point set of the mechanism's singular position at this height is increased. However, with the increase of the lifting platform's height, the point set of the mechanism's singular position decreases significantly.

Figures 17 and 18 show the singular image when the kinematic parameters of the moving platform z_p are equal to 190 mm and 210 mm, and the value range of L_4 is [60,100] mm. Research shows that when L_4 is a fixed value, as the value of the kinematic parameter z_p of the moving platform increases, the mechanism's singular

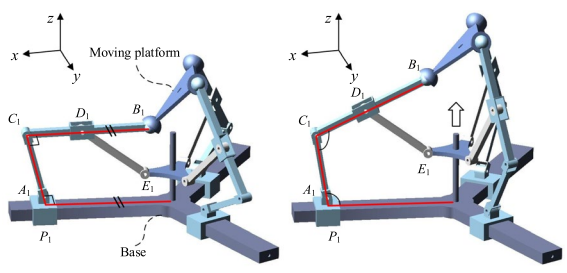

(a) Singular position 1 of mechanism (b) Avoiding singularity

Figure 20 Increasing the height of the lifting platform to avoid singularity at the singular position 1

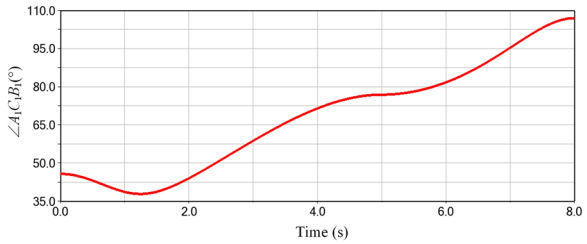

Figure 21 The simulation value of $\angle A_1C_1B_1$ when the mechanism avoids singular position 1

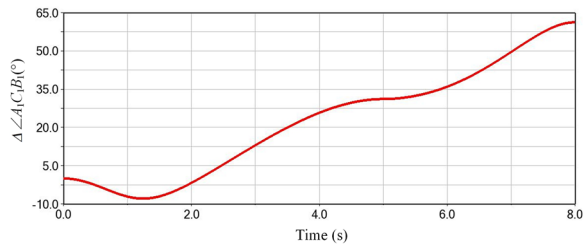

Figure 22 The variation of $\angle A_1C_1B_1$ when the mechanism avoids singular position 1 (The symbol " Δ "represents the variation of the angle)

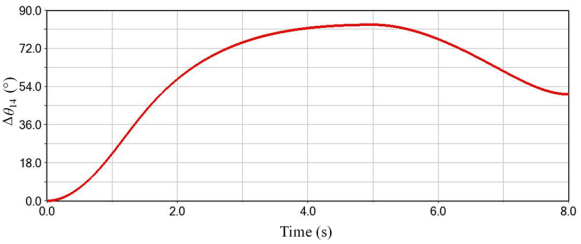

Figure 23 The variation of θ_{14} when the mechanism avoids singular position 1

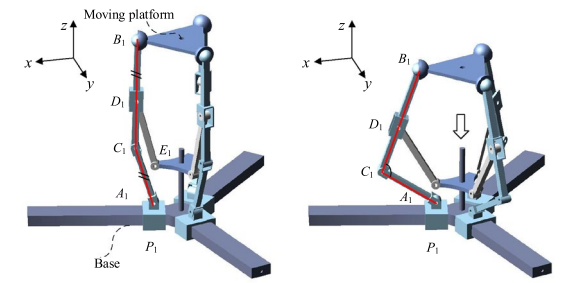

(a) Singular position 2 of mechanism (b) Avoiding singularity

Figure 24 Decreasing the height of the lifting platform to avoid singularity at the singular position 2

position will continue to increase. Similarly, the change of the lifting platform's height value will affect the number of point sets of the singular positions.

Research shows that the change of the kinematic parameters of redundant components has an obvious influence on the mechanism's singular performance. When the moving platform is at a certain height, the lifting platform's height change will reduce the singular position of the mechanism. It also shows that in this 3-DOF parallel mechanism, the addition of redundant components will positively affect the kinematics of the mechanism. When the mechanism is in a singular position, the mechanism's posture can be changed by changing the height of the lifting platform so as to avoid singularity.

4 Simulation Analysis

4.1 Simulations of Mechanism Avoiding Singular Position Under Three Actions

In the previous section, it has been found that the 3-DOF PM-KR has the characteristics of avoiding singularity. When the mechanism is in singular positions, it can avoid the singular positions by changing the lifting platform's height. In this section, the Adams software is used to simulate the three singular positions of the mechanism. By changing the height of the lifting platform,

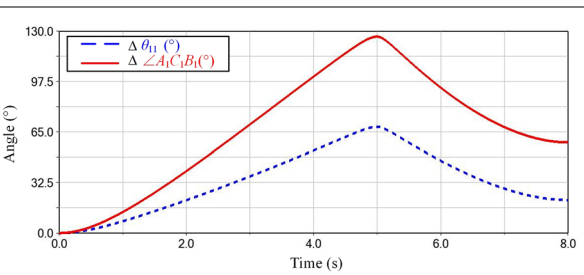

Figure 25 The variation of θ_{11} and $\angle A_1C_1B_1$ when the mechanism avoids singular position 2

the singular position of the mechanism can be avoided, which can verify the kinematic characteristics of the mechanism.

The mechanism's initial position is shown in Figure 19. The height of the moving platform $z_p = 170$ mm, the deflection angle $\alpha = \beta = 0°$, the height of the lifting platform $L_4 = 60$ mm, and the three actuating parameters on the base $L_1 = L_2 = L_3 = 135$ mm.

As shown in Figure 20a, take limb 1 as an example, it is the first singular position of the mechanism, and the actuating joint's positions are $L_1 = 215$ mm, $L_2 = L_3 = 100$ mm, and $L_4 = 60$ mm. At this time, θ_{11} is approximately equal to 90°, the link A_1C_1 of limb 1 is

approximately perpendicular to the base, the link C_1B_1 is approximately parallel to the base, and the moving platform occurs a large angle. To avoid this singular position, we can increase the height of the lifting platform. When L_4 is equal to 100 mm, the position and posture of the mechanism change, so as to the mechanism can avoid the singular position, as shown in Figure 20b. Similarly, when such singularity occurs in limb 2 or limb 3, it can also be avoided by adjusting the height of the lifting platform.

In the first stage of the simulation, the mechanism moves from the initial position to the singular position 1, the simulation time is 0–5 s; the second stage is the process of avoiding the singular positions of the mechanism, and the simulation time is 5–8 s. In the simulation using Adams software, the rotation angle of the moving platform, revolving joint and spherical joint are measured to judge whether the mechanism completes the action of avoiding singular positions.

As shown in Figure 21, it is the simulation value of $\angle A_1C_1B_1$ of the mechanism. At the 5th second, indicate that link A_1C_1 and link C_1B_1 are approximately perpendicular at this time. At this time, the mechanism is close to the singular position, and link A_1C_1 and link C_1B_1 are close to vertical. If the position of the lifting platform does not change, the mechanism will be singular. By changing the height of the lifting platform, the mechanism can avoid the singular position. When the position of the lifting platform increases, the angle between the two links changes. $\angle A_1C_1B_1$ is greater than 90° and keeps increasing, which shows that the result of avoiding singular positions is obvious.

The rotation angle of the spherical joint B_1 in the *xoz* plane is set as θ_{14}. Figures 22 and 23 show the variation of $\angle A_1C_1B_1$ and θ_{14} respectively. At the 5th second, the variation of $\angle A_1C_1B_1$ is approximately 31.15°. After the 5th second, as the lifting platform's height increases, the variation of $\angle A_1C_1B_1$ gradually increases. At the 8th second, the amount is 61.26°. The variation of θ_{14} gradually

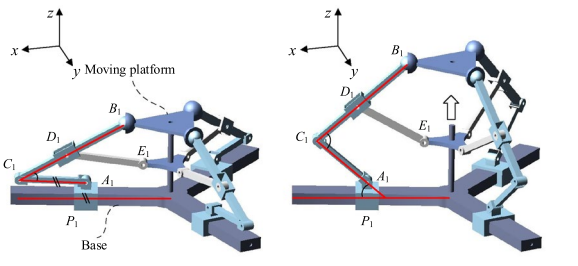

(a) Singular position 3 of mechanism (b) Avoiding singularity

Figure 26 Increasing the height of the lifting platform to avoid singularity at the singular position 3

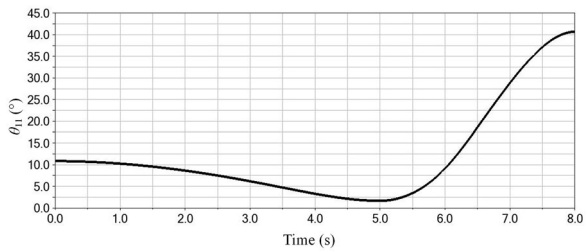

Figure 27 The simulation value of θ_{11} when the mechanism avoids singular position 3

increases until the mechanism reaches the singular position. Then it decreases as the lifting platform's height increases, which indicates that the mechanism avoids singularity and returned to its normal position and posture.

When θ_{i1} and θ_{i2} of the mechanism are approximately equal to 90°, it is the singular position 2 of the mechanism. The actuating joint's positions are $L_1 = L_2 = L_3 =$ 100 mm and $L_4 = 100$ mm, the link l_{i1} and link l_{i3} of the three limbs are approximately perpendicular to the base, as shown in Figure 24a. By decreasing the height of the lifting platform, the mechanism can avoid singularity. When $L_4 = 60$ mm, the posture of the limb changes and the height of the moving platform decreases simultaneously, and the mechanism returns to its normal posture, as shown in Figure 24b.

As shown in Figure 25, it is the variation of θ_{11} and $\angle A_1C_1B_1$ when the mechanism avoids singular position 2. At the 5th second, the variation of θ_{11} and $\angle A_1C_1B_1$ reach their maximum values of 68.34° and 126.45°. If the three actuating joints of the mechanism continue to move forward, θ_{11} will continue to increase, and $\angle A_1C_1B_1$ will continue to decrease, so the mechanism will reach the singular position. By decreasing the height of the lifting platform, link l_{i2} can change the position of link l_{i1} and link l_{i3}, which can change the overall posture of the mechanism. If θ_{i1} and θ_{i2} are less than 90° and keep decreasing, it is proved that the mechanism can avoid singular position 2.

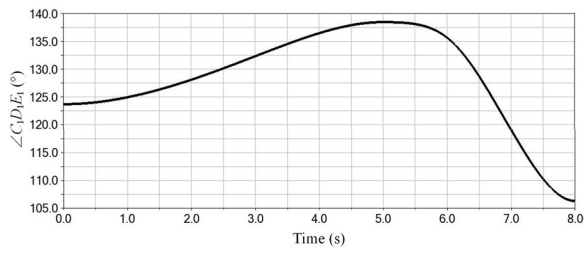

Figure 28 The simulation value of $\angle C_1D_1E_1$ when the mechanism avoids singular position 3

After 5 s, the lifting platform's height decreases, and the variation of θ_{11} and $\angle A_1C_1B_1$ are reduced to 21.28° and 58.27° respectively, which indicates that the mechanism has avoided the singular positions.

When the angle θ_{i1} is approximately equal to 0°, the third singular position of the mechanism occurs. The actuating joint's positions are $L_1 = L_2 = L_3 = 143$ mm and $L_4 = 60$ mm, and the link l_{i1} of the three limbs is approximately parallel to the base, as follows, as shown in Figure 26a. By increasing the height of the lifting platform, the mechanism can avoid singularity. When $L_4 =$ 100 mm, the moving platform's height is increased, and the overall posture of the mechanism changes.

Figures 27 and 28 show the simulation values of θ_{11} and $\angle C_1D_1E_1$ when the mechanism avoids singular position 3. At the 5th second, the value of θ_{11} is 1.66°, close to 0°, which indicates that link l_{i1} is approximately parallel to the base at this position. If the actuating joint continues to move, the mechanism will be singular. At this time, by increasing the height of the lifting platform, the position of the link l_{i2} will move and the position of the link l_{i1} and the link l_{i3} will be changed. If θ_{11} increases, $\angle C_1D_1E_1$ will decrease, proving that the mechanism can avoid singular positions. After 5 s, increasing the height of the lifting platform, θ_{11} significantly increases to 40.68°, and $\angle C_1D_1E_1$ also changes significantly, which can indicate that the height of the lifting platform makes the mechanism successfully avoid the singularity.

4.2 Discussion

It is proved that the singularities can be avoided by changing the lifting platform's height when the mechanism is near or already in the singular positions. It also shows that the redundant kinematics part significantly improves the mechanism's kinematics performance and proves that the 3-DOF PM-KR has the advantages of structural design.

However, there are some problems in the simulation research. For example, the simulation of the mechanism is too ideal and doesn't fully consider the influence of the errors of the mechanism's materials and joints on the simulation results; when the mechanism reaches different singular positions, the force and deformation between joints and links will affect the overall mechanism. The parameters changing of the mechanism will also affect the effect of avoiding singular positions. In the follow-up research, we should solve these known problems as much as possible.

5 Conclusions

In this paper, the kinematics performance of a 3-DOF PM-KR and the influence of redundant parts on the mechanism are analyzed. The conclusions are drawn as follows:

(1) Through the analysis of the inverse kinematics of the PM-KR, it can be concluded that different actuating parameters of kinematic redundancy lead to different solutions. Since there are infinite solutions for the inverse kinematics of PM-KR, the actuating parameter of kinematic redundancy should be set as a constant firstly.
(2) When the parameter of the redundant part is increased, the singularity of the mechanism can be significantly reduced. This proves that the kinematic redundancy affects the workspace and singularity of the 3-DOF PM-KR.
(3) Due to the existed kinematic redundancy, the PM-KR possesses the characteristic of fault tolerance. When the position of the failed actuating joint is far away from the center, the fault-tolerant performance of the PM-KR is better.

Acknowledgements
Not applicable.

Author contributions
CS wrote the manuscript; HQ was in charge of the whole trial, review and edition; SG and XL assisted with review. All authors read and approved the final manuscript.

Authors' Information
Chaoyu Shen, born in 1995, is currently an engineer at *China Waterborne Transport Research Institute*, *China*. He received his master degree on mechanical design and theory from *School of Mechanical, Electronic and Control Engineering*, *Beijing Jiaotong University*, *China*, in 2021. His research interests include robotics mechanism and parallel robots.
Haibo Qu, born in 1983, is currently an associate professor in *School of Mechanical, Electronic and Control Engineering*, *Beijing Jiaotong University*, *China*. He received his PhD degree in mechanical design and theory from *Beijing Jiaotong University, China*, in 2013. His research interests include robotics mechanism and mechatronics.
Sheng Guo, born in 1972, is currently a full professor, a vice director of *Robotics Research Center*, *Beijing Jiaotong University* and a dean of *School of Mechanical, Electronic and Control Engineering*, *Beijing Jiaotong University*, *China*. He received his PhD degree from *Beijing Jiaotong University*, *China*, in 2005. His research interests include robotics mechanism and mechatronics.
Xiao Li, born in 1995, is currently a PhD candidate at *School of Mechanical, Electronic and Control Engineering*, *Beijing Jiaotong University*, *China*. She received her bachelor degree from *Beijing Jiaotong University, China*, in 2019. Her research interests include parallel robots with kinematic redundancy.

Funding
Supported by Fundamental Research Funds for the Central Universities (Grant No. 2022JBZX025), Natural Science Foundation of Hebei Province (Grant No.

E2022105029) and National Natural Science Foundation of China (Grant No. 51875033).

Competing Interests
The authors declare no competing financial interests.

Author Details
[1]Robotics Research Center, School of Mechanical, Electronic and Control Engineering, Beijing Jiaotong University, Beijing 100044, China. [2]China Waterborne Transport Research Institute, Beijing 100088, China. [3]Key Laboratory of Vehicle Advanced Manufacturing, Measuring and Control Technology, Ministry of Education, Beijing Jiaotong University, Beijing 100044, China.

Received: 25 October 2021 Revised: 16 May 2022 Accepted: 5 August 2022
Published online: 05 September 2022

References

[1] F A Wen, G Yang. Overview of parallel robot mechanisms. *Mechanical Science and Technology*, 2000, 19(1): 69-72 (in Chinese).
[2] J P Merlet. Redundant parallel manipulators. *Laboratory Robotics and Automation*, 2015, 8(1): 17-24.
[3] G F Liu, Y L Wu, X Z Wu, et al. Analysis and control of redundant parallel manipulators. *IEEE International Conference on Robotics and Automation*, 2001, 4: 3748-3754.
[4] H B Liao, T M Li, X Q Tang. Singularity analysis of redundant parallel manipulators. *2004 IEEE International Conference on Systems*, 2004, 5: 4214-4220.
[5] F Q Zhao, S Guo, Z C Xu, et al. Design and analysis of high-performance machine tools based on redundant parallel mechanisms. *Journal of Central South University (Science and Technology)*, 2019, 50(1): 67-74 (in Chinese).
[6] C X Yan, Q Zhan, Z Lu. Fault-tolerant method of parallel robot based on drive or structure redundancy. *Journal of Beijing University of Aeronautics and Astronautics*, 2010, 36(12): 1407-1411 (in Chinese).
[7] X M Wang, G H Cui, H J Hou, et al. Research on kinematic statics and singularity of redundant drive 2SPR-2RPU parallel mechanism. *Chinese Journal of Engineering Design*, 2019, 26(5): 619-626 (in Chinese).
[8] C T Chen , H V Pham. Trajectory planning in parallel kinematic manipulators using a constrained multi-objective evolutionary algorithm. *Nonlinear Dynamics*, 2012, 67(2): 1669-1681.
[9] H Saafi, H Lamine. Comparative kinematic analysis and design optimization of redundant and nonredundant planar parallel manipulators intended for haptic use. *Robotica*, 2020, 38(8): 1463-1477.
[10] N Bahman, M Farid, M Mahzoon. Redundancy resolution and control of a novel spatial parallel mechanism with kinematic redundancy. *Mechanism and Machine Theory*, 2018, 133: 112-126.
[11] Y P Lang, et al. Optimization design for a compact redundant hybrid parallel kinematic machine. *Robotics and Computer-Integrated Manufacturing*, 2019, 58: 172-180.
[12] K F Wen, C Gosselin. Forward kinematic analysis of kinematically redundant hybrid parallel robots. *Journal of Mechanisms and Robotics*, 2020, 12(6): 1-11.
[13] K F Wen, C Gosselin. Exploiting redundancies for workspace enlargement and joint trajectory optimization of a kinematically redundant hybrid parallel robot. *Journal of Mechanisms and Robotics*, 2021, 13(4): 040905.
[14] J Landuré, C Gosselin. Kinematic analysis of a novel kinematically redundant spherical parallel manipulator. *Journal of Mechanisms and Robotics*, 2018, 10(2): 1-10.
[15] M Isaksson, C Gosselin, K Marlow. Singularity analysis of a class of kinematically redundant parallel Schönflies motion generators. *Mechanism and Machine Theory*, 2017, 112: 172-191.
[16] H B Qu, S Guo, Y Zhang. A novel relative degree-of-freedom criterion for a class of parallel manipulators with kinematic redundancy and its applications. *Proceedings of the Institution of Mechanical Engineers*, *Part C*: *Journal of Mechanical Engineering Science*, 2016, 231(22): 4227-4240.
[17] H B Qu, C L Zhang, S Guo. Structural synthesis of a class of kinematically redundant parallel manipulators based on modified G–K criterion and RDOF criterion. *Mechanism and Machine Theory*, 2018, 130: 47-70.
[18] H B Qu, Y F Fang, S Guo. Structural synthesis and analysis of a class of wrist mechanisms with redundantly-actuating closed-loop units. *Proceedings of the Institution of Mechanical Engineers*, *Part C*: *Journal of Mechanical Engineering Science*, 2016, 230(2): 276-290.
[19] Y Q Li, Y Zhang, L J Zhang. A new method for type synthesis of 2R1T and 2T1R 3-DOF redundant actuating parallel mechanisms with closed loop units. *Chinese Journal of Mechanical Engineering*, 2020, 33: 78.
[20] Q M Wang, J Su, et al. Structural characteristics and kinematics analysis of a redundant 6-DOF parallel mechanism. *Journal of Mechanical Engineering*, 2017, 53(18): 121-130. (in Chinese)
[21] J Wang, C Gosselin. Kinematic analysis and design of kinematically redundant parallel mechanisms. *Journal of Mechanical Design,* 2004, 126(1): 109-118.
[22] B Q Xu, T M Li, X J Liu, et al. Workspace analysis of the 4RRR planar parallel manipulator with actuation redundancy. *Tsinghua Science and Technology*, 2010, 15(5): 509-516.
[23] L T Schreiber, C Gosselin. Schnflies motion parallel robot (SPARA): A kinematically redundant parallel robot with unlimited rotation capabilities. *IEEE/ASME Transactions on Mechatronics*, 2019, 24(5): 2273-2281.
[24] H B Qu, L Q Hu, S Guo. Singularity analysis and avoidance of a planar parallel mechanism with kinematic redundancy under a fixed orientation. *Proceedings of the Institution of Mechanical Engineers*, *Part C*: *Journal of Mechanical Engineering Science*, 2021, 235(18): 3534-3553.
[25] Y M Zhao, Z L Jin. Optimum design of wave energy conversion device based on 3-RPS/3-SPS parallel mechanism with redundant branches. *Journal of Mechanical Engineering*, 2019, 55(23): 93-102. (in Chinese)
[26] X D Jin, Y F Fang, D Zhang. Design and analysis of a class of redundant collaborative manipulators with 2D large rotational angles. *Frontiers of Mechanical Engineering*, 2020, 15(1): 66-80.
[27] M Z Huang, J T Thebert. A study of workspace and singularity characteristics for design of 3-DOF planar parallel robots. *International Journal of Advanced Manufacturing Technology*, 2020, 51: 789-797.
[28] H B Qu, L Q Hu, S Guo, et al. Static analysis of a planar parallel mechanism with kinematic redundancy and closed-loop limb. *Journal of Central South University (Science and Technology)*, 2020, 51(10): 2758-2771.
[29] N R A Bahman, M Mahzoon, M Farid. Singularity-free trajectory planning of a 3-RPRR planar kinematically redundant parallel mechanism for minimum actuating effort. *Iranian Journal of Science and Technology Transactions of Mechanical Engineering*, 2018, 43: 739-751.
[30] L T Schreiber, C Gosselin. Kinematically redundant planar parallel mechanisms: Kinematics, workspace and trajectory planning. *Mechanism and Machine Theory*, 2018, 119: 91-105.
[31] N Baron, A Philippides, N Rojas. A robust geometric method of singularity avoidance for kinematically redundant planar parallel robot manipulators. *Mechanism and Machine Theory*, 2020, 151(1): 103863
[32] M Slavutin, A Sheffer, Y Reich, et al. A novel criterion for singularity analysis of parallel mechanisms. *Mechanism and Machine Theory*, 2019, 137: 459-475.
[33] X L Yang, H T Wu, B Chen, et al. A dual quaternion approach to efficient determination of the maximal singularity-free joint space and workspace of six-DOF parallel robots. *Mechanism and Machine Theory*, 2018, 129: 279-292.
[34] Z Zhang, Z Shao, F Peng, et al. Workspace analysis and optimal design of a translational cable-driven parallel robot with passive springs. *Journal of Mechanisms and Robotics*, 2020, 12(5): 1-31.
[35] A L Orekhov, N Simaan. Directional stiffness modulation of parallel robots with kinematic redundancy and variable stiffness joints. *Journal of Mechanisms and Robotics*, 2019, 11(5): 1-14.
[36] A H Dastjerdi, M M Sheikhi, M T. Masouleh. A complete analytical solution for the dimensional synthesis of 3-DOF delta parallel robot for a prescribed workspace. *Mechanism and Machine Theory*, 2020, 153:103991.